Cell Reports

Article

SH3Ps recruit auxilin-like vesicle uncoating factors for clathrin-mediated endocytosis

Graphical abstract

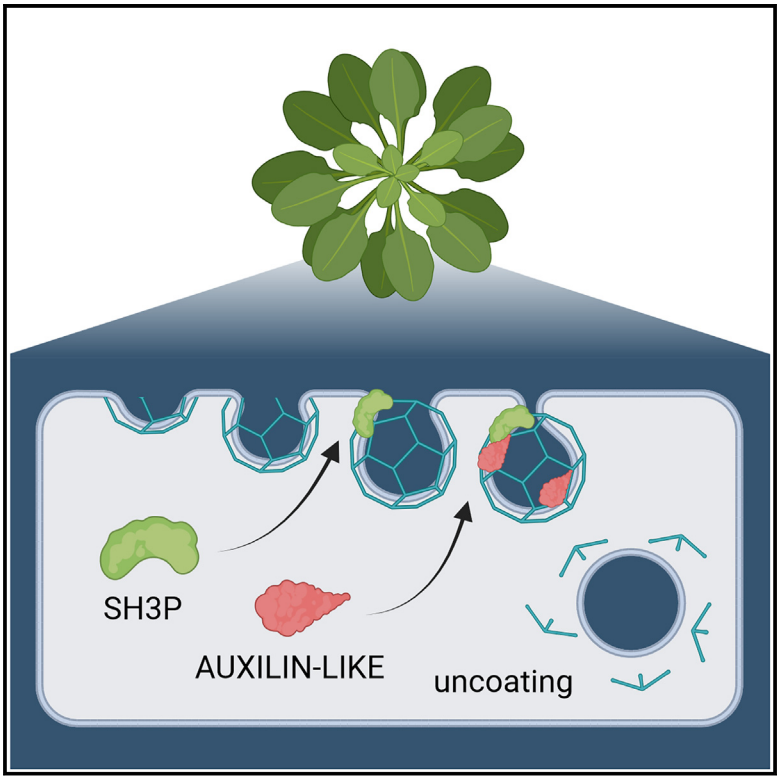

Authors

Maciek Adamowski, Marek Randuch, Ivana Matijević, Madhumitha Narasimhan, Jiří Friml

Correspondence

jiri.friml@ist.ac.at

In brief

Clathrin-mediated endocytosis is a universal process in eukaryotes, but studies reveal unique aspects of its molecular mechanism in distinct lineages. Adamowski et al. report a plant-specific interaction module in clathrin-mediated endocytosis where conserved BAR-SH3 proteins recruit auxilin-like uncoating factors to vesicles.

Highlights

- SH3Ps are endocytic BAR-SH3 domain proteins in *Arabidopsis thaliana*
- SH3P2 binds to clathrin-coated vesicles before scission and uncoating
- SH3Ps recruit auxilin-like vesicle uncoating factors to the plasma membrane
- SH3Ps support clathrin-mediated endocytosis in concert with the TPLATE complex

Adamowski et al., 2024, Cell Reports *43*, 114195
May 28, 2024
https://doi.org/10.1016/j.celrep.2024.114195

CellPress

Cell Reports

CellPress
OPEN ACCESS

Article

SH3Ps recruit auxilin-like vesicle uncoating factors for clathrin-mediated endocytosis

Maciek Adamowski,[1,2] Marek Randuch,[1] Ivana Matijević,[1] Madhumitha Narasimhan,[1] and Jiří Friml[1,3,*]
[1]Institute of Science and Technology Austria, Am Campus 1, 3400 Klosterneuburg, Austria
[2]Plant Breeding and Acclimatization Institute – National Research Institute, Radzików, 05-870 Błonie, Poland
[3]Lead contact
*Correspondence: jiri.friml@ist.ac.at
https://doi.org/10.1016/j.celrep.2024.114195

SUMMARY

Clathrin-mediated endocytosis (CME) is an essential process of cargo uptake operating in all eukaryotes. In animals and yeast, BAR-SH3 domain proteins, endophilins and amphiphysins, function at the conclusion of CME to recruit factors for vesicle scission and uncoating. *Arabidopsis thaliana* contains the BAR-SH3 domain proteins SH3P1–SH3P3, but their role is poorly understood. Here, we identify SH3Ps as functional homologs of endophilin/amphiphysin. SH3P1–SH3P3 bind to discrete foci at the plasma membrane (PM), and SH3P2 recruits late to a subset of clathrin-coated pits. The SH3P2 PM recruitment pattern is nearly identical to its interactor, a putative uncoating factor, AUXILIN-LIKE1. Notably, SH3P1–SH3P3 are required for most of AUXILIN-LIKE1 recruitment to the PM. This indicates a plant-specific modification of CME, where BAR-SH3 proteins recruit auxilin-like uncoating factors rather than the uncoating phosphatases, synaptojanins. SH3P1–SH3P3 act redundantly in overall CME with the plant-specific endocytic adaptor TPLATE complex but not due to an SH3 domain in its TASH3 subunit.

INTRODUCTION

Endocytosis is a process at the plasma membrane (PM) leading to the internalization of surface proteins and other cargo. In plants, as in other eukaryotes, the most common mode of endocytosis is a vesicular transport process involving the vesicle coat protein clathrin.[1,2] Clathrin-mediated endocytosis (CME) has been studied in detail in animals and yeast,[3] where it was described as a process of high complexity involving, beyond clathrin, a large array of other protein factors.[4] These perform functions that include binding clathrin with the membrane, force generation for membrane bending, and selective loading of cargo at earlier stages. At late stages of CME, specialized factors mediate the separation of the completed vesicle from the PM and uncoating; i.e., removal of the protein coat to release the vesicle for fusion with an endosomal compartment.

In non-plants, the formation of clathrin-coated vesicles (CCVs), especially the late steps leading to scission and uncoating, involves the action of BAR (Bin, amphiphysin, and Rvs) domain proteins.[5,6] BAR domains are dimers forming structures of a crescent shape, which typically bind membranes through concave surfaces displaying positive charges. Therefore, BAR domains act as curvature sensors, binding, for instance, to narrow necks of nearly formed CCVs, and as curvature generators, where their binding and polymerization leads to further membrane bending. CME involves a suite of BAR domain proteins with distinct recruitment characteristics and composition beside the BAR domain.[7,8] Notable examples are amphiphysins and endophilins, which possess an SH3 domain, an interaction module with affinity for proline-rich sequences on protein targets.[9] The SH3 domains of amphiphysins and endophilins interact with dynamins, mechanoproteins acting in vesicle scission, and with synaptojanins, phospholipid phosphatases that promote uncoating by modifying vesicle membrane lipid composition.[10–12] Thus, thanks to the curvature-sensing properties of BAR domains and the interactions of SH3 domains, BAR-SH3 proteins act as binding intermediates, enabling a temporally regulated activity of factors needed for the final steps of CME.[13–16]

The characterization of CME in *Arabidopsis thaliana*, including the steps leading to scission and uncoating, is less advanced.[17] *A. thaliana* contains three proteins with a BAR-SH3 domain composition similar to non-plant endophilin/amphiphysin, SH3P1–SH3P3 (SH3 DOMAIN-CONTAINING PROTEIN1–3). In support of a conserved function, expression of SH3P1–SH3P3 partially complements the yeast amphiphysin mutant *rvs167*.[18] Physical binding between SH3P1–SH3P3 and plant dynamins was detected.[19–21] SH3P2 also interacts with SAC9 (SUPPRESSOR OF ACTIN9), which may have a synaptojanin-like activity in the endocytic pathway in *A. thaliana*.[22] Interestingly, SH3Ps also physically interact with some of the putative *A. thaliana* homologs of auxilin, a class of uncoating factors that act by the recruitment of Hsc70 (heat shock cognate 70), causing relaxation of the clathrin cage in mammals.[23] The

homologous AUXILIN-LIKE1 and AUXILIN-LIKE2 possess Pro-rich domains, and interactions with specific SH3P isoforms were detected by yeast two-hybrid assay, co-immunoprecipitation, bimolecular fluorescence complementation, and their common isolation in tandem affinity purification with CLATHRIN LIGHT CHAIN (CLC) as bait.[18,22,24] These interactions may represent a plant-specific modification of CME, where BAR-SH3 proteins engage with auxilin-like uncoating factors to promote CCV uncoating,[18] but consequences of this model have not been explored *in planta*. Overall, a comprehensive evaluation of the role of SH3P1–SH3P3 in CME, indicated also by the identification of SH3P1 and SH3P2 in the proteome of purified CCVs[25] and by the coimmunoprecipitation of SH3P2 with CLATHRIN HEAVY CHAIN (CHC),[26] is lacking. That said, functions such as trafficking of ubiquitinated cargoes and a role in autophagy and in cell plate formation have been assigned to SH3P2.[20,26–28]

Here, with the use of loss-of-function and advanced live-imaging approaches, we characterize the role of SH3P1–SH3P3 in CME and explore their connections with the putative uncoating factors AUXILIN-LIKE1/2. Our results demonstrate a role of SH3P1–SH3P3 as homologs of endophilin/amphiphysin, which engage in a plant-specific association with auxilin-like uncoating factors. Interestingly, SH3P1–SH3P3 are functionally redundant with the endocytic adaptor TPLATE complex (TPC), but this is not due to the presence of an SH3 domain in one of its subunits. Together, this study contributes to the ongoing characterization of the unique properties of CME, which evolved in the plant lineage.

RESULTS

Isolation and complementation of *sh3p123* mutants

The literature reports variably on the effects of SH3P1–SH3P3 deficiency. Multiple *sh3p* mutant combinations, with transfer DNA (T-DNA) alleles that are likely not full knockouts, did not exhibit obvious phenotypic defects.[20,26] In turn, an RNA interference (RNAi) line silencing *SH3P2* exhibited an arrest of seedling development,[27] indicating an essential and non-redundant function of SH3P2, but this was not reproduced with a similar artificial microRNA (amiRNA) line.[26]

To clarify the function of SH3P1–SH3P3, we isolated *sh3p123* triple mutants using CRISPR-Cas9-generated mutations in the exons of *SH3P1* and *SH3P2* and an exon T-DNA insertion in *SH3P3,* all of which disrupt coding sequences, producing null alleles (Figure S1A; Table S1). Predicted mutant proteins terminate early in the N-terminal BAR domains (Figure S1B; Data S1). We obtained two independent triple-homozygous mutant allele combinations, $sh3p123^{9C}$ and $sh3p123^{10G}$. The triple knockouts exhibited reduced growth as seedlings (Figure 1A) as well as adults (Figures 1B, S2A, and S2B). These mutant phenotypes were absent from *sh3p12* and *sh3p3* (Figures S2C and S2D), indicating a functional redundancy of the three isoforms. We complemented the triple mutant by transforming $sh3p123^{10G}$ with $35S_{pro}$*:SH3P1-GFP*, $35S_{pro}$*:SH3P2-GFP*, and $35S_{pro}$*:SH3P3-GFP*. Expression of any of the three fusion proteins successfully complemented the mutant, to a varied degree in individual transgenic lines and specimen, at adult (Figures 1C and S3A) and seedling (Figure S3B) stages of development. The triple mutant complementation by each isoform confirms that the three isoforms possess a redundant function, and shows functionality of C-terminal fluorescent protein fusions; variability in the degree of complementation may be a result of transgene silencing and variable transgene expression levels.

Taken together, knockout mutants and their complementation indicate that SH3P1–SH3P3 possess a redundant function supporting growth and development.

Normal CME in the absence of SH3P1–SH3P3

To test the requirement of SH3P1–SH3P3 for CME, we crossed $sh3p123^{10G}$ with $CLC2_{pro}$*:CLC2-GFP* $UBQ10_{pro}$*:mCherry-AUXILIN-LIKE1* reporter line. We evaluated CME by total internal reflection fluorescence (TIRF) microscopy of CLC2-GFP, a clathrin coat marker. Measured either in the epidermis of the early elongation zones of seedling roots (Figure 2A) or in the epidermis of etiolated hypocotyls (Figure 2B), the densities of clathrin-coated pits (CCPs) at the PMs were equal in the wild type and the mutant, indicative of normal CME rates in the absence of SH3P1–SH3P3. To evaluate the dynamics of single endocytic vesicle formation events, we measured persistence times of individual clathrin-positive structures captured on TIRF time-lapses in the hypocotyl. The lifetime distribution of CCV formation events in $sh3p123^{10G}$ was very similar to the wild type (Figure 2C), also indicating that CME occurs normally in the mutant. As a further assessment of endocytosis, we performed uptake experiments with the membrane dye FM4-64[29–31] in seedling root apical meristems (RAMs) of $sh3p123^{9C}$ and $sh3p123^{10G}$. After 15 min of FM4-64 uptake, the intracellular signals of FM4-64 relative to signal levels at the PM were normal in both triple-mutant alleles (Figure 2D), further confirming normal endocytosis in the absence of SH3P1–SH3P3. Furthermore, as a proxy for endocytosis, we evaluated the accumulation of the PIN1 auxin transporters in BFA (brefeldin A) bodies (i.e., endomembrane aggregations forming in *A. thaliana* upon treatments with the ARF-GEF [ADP ribosylation factor guanine nucleotide exchange factor] inhibitor BFA)[32,33] and similarly found a normal accumulation of PIN1 in both mutant alleles, not indicative of a defective CME of PIN1 (Figures 2E and S4).

In summary, both direct and indirect measurements indicate that CME is normal in the absence of SH3P1–SH3P3.

Localization of SH3P1–SH3P3 at the PM and recruitment to CCPs

Subcellular localization data places SH3P2-GFP at the PM and at cell plates, on endomembrane structures, and on autophagosomes.[20,24,26,27] The association of SH3P2 with the PM is mediated by the BAR domain[26] and depends on phosphatidylinositol 4,5-bisphosphate.[34] We evaluated the localization of all three SH3Ps using functional SH3P-GFP fusions expressed in complemented $sh3p123^{10G}$. Observed with confocal laser scanning microscopy (CLSM) in the seedling RAM, all three isoforms localized to the PM and cytosol (Figures 3A and S5A). Only SH3P2-GFP, but not SH3P1-GFP or SH3P3-GFP, often additionally localized to intracellular structures (Figures 3A and S5A) similar to those observed in a previously generated $UBQ10_{pro}$*:SH3P2-GFP* line (Figure S5B). During cell division, all three fluorescent

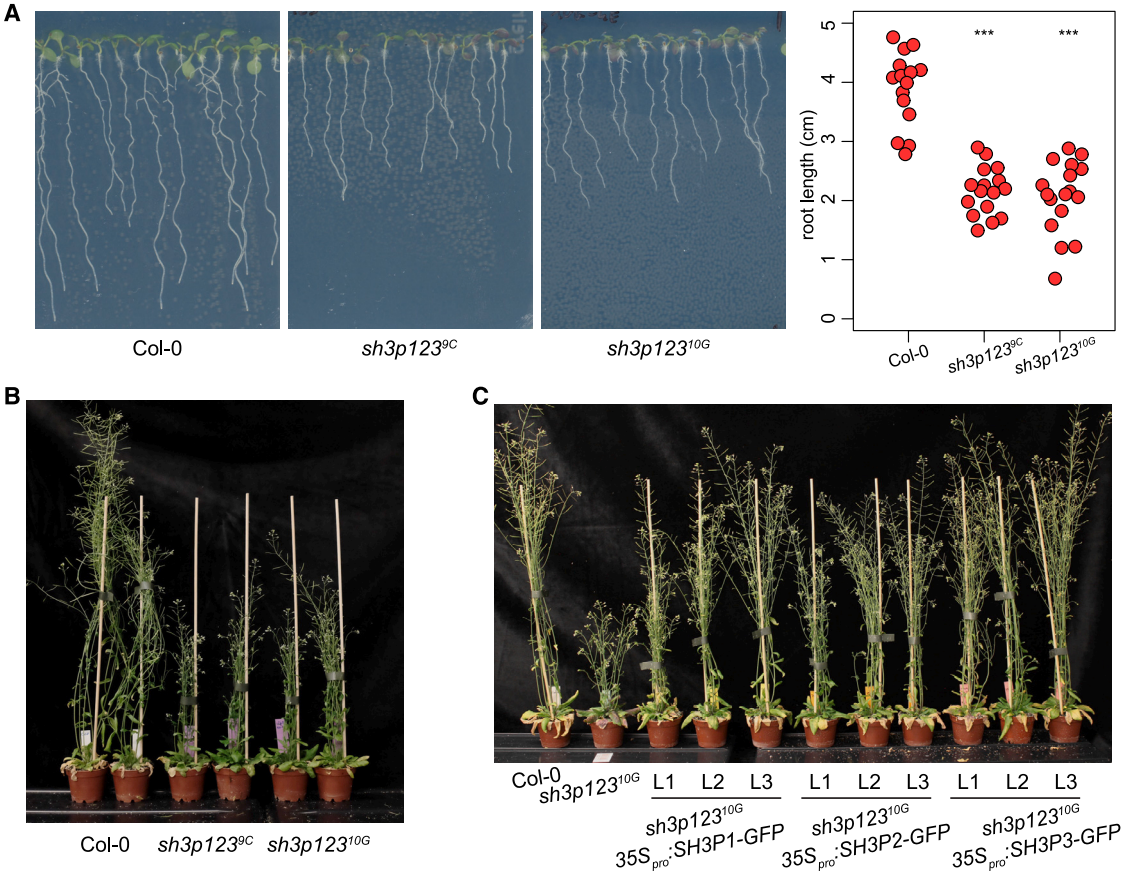

Figure 1. *sh3p123* loss of function mutants

(A and B) Seedling (A) and adult (B) development of *sh3p123* knockout mutants. Two independently obtained allele combinations are shown. *sh3p123* mutants are characterized by a reduced growth of seedlings and adults. The graph in (A) shows main root lengths of individual seedlings after 7 days of *in vitro* growth from a representative experiment (3 replicates). Col-0: 3.90 ± 0.62 cm (mean ± SD), $n = 15$; $sh3p123^{9C}$: 2.16 ± 0.41 cm, $n = 16$; $sh3p123^{10G}$: 2.07 ± 0.61 cm, $n = 17$. Mutant values were compared with the wild type using t tests, $p < 0.0001$. See also Figures S1 and S2 and Data S1.

(C) Complementation of $sh3p123^{10G}$ with $35S_{pro}$:*SH3P1-GFP*, $35S_{pro}$:*SH3P2-GFP*, and $35S_{pro}$:*SH3P3-GFP* constructs. Single plants from three independent transgenic lines carrying each construct are shown. All three constructs complement the mutant phenotype with varying degrees in individual lines.

See also Figure S3.

protein fusions localized to cell plates (Figure S5C). TIRF imaging of the PM localization patterns of all three isoforms showed relatively sparse, clear fluorescent foci of signal (Figure 3B, top). The lifetimes of individual foci at the PM varied significantly, from foci existing briefly (2–3 s) up to signals persisting for over 100 s (Figures 3B, bottom; S6A).

To assess whether SH3P1–SH3P3 localize at CCPs, we generated a double marker line, $UBQ10_{pro}$:*SH3P2-GFP* $RPS5A_{pro}$:*CLC2-mRuby*, and conducted TIRF time-lapse imaging in the early elongation zone of the root and in etiolated hypocotyls. In both tissues, we found SH3P2-GFP traces associated with a subset of CCPs marked by CLC2-mRuby, where SH3P2-GFP was recruited at the final stage of CCP formation that leads to the detachment of the CCV from the PM (Figures 3C and 3D, yellow arrowheads). This recruitment of SH3P2-GFP to CCVs around the time of their detachment could be followed most clearly in instances where the CCV departed from the PM in plane of a kymograph section, producing a "hockey stick" pattern (Figures 3C and S6B). The observation of SH3P2-GFP signals coinciding exactly with departing CCVs ascertained that the captured events of colocalization represented genuine instances of SH3P2-GFP recruitment to CCVs rather than incidental, random overlaps of fluorescent signals. The persistence time of SH3P2-GFP on these detaching CCVs ranged between 2 and 8 s. This colocalization pattern indicates a function of SH3P1–SH3P3 at final stages of CCP formation during scission and/or uncoating, similarly to endophilins and amphiphysins.[7] However, this activity occurs only on a subset of all forming CCVs, as many CCP formation events did not involve SH3P2-GFP (Figures 3C and 3D, white arrowheads). Conversely, SH3P2-GFP often localized to the PM at sites not containing clathrin (Figures 3C and 3D, blue arrowheads).

Taken together, fluorescent live imaging of SH3P1–SH3P3 shows their dynamic localization to distinct spots at the PM, and colocalization of SH3P2-GFP with clathrin indicates their late recruitment to a subpopulation of CCPs, suggestive of a potential function in late stages of CME, similar to endophilin and amphiphysin in non-plant systems.

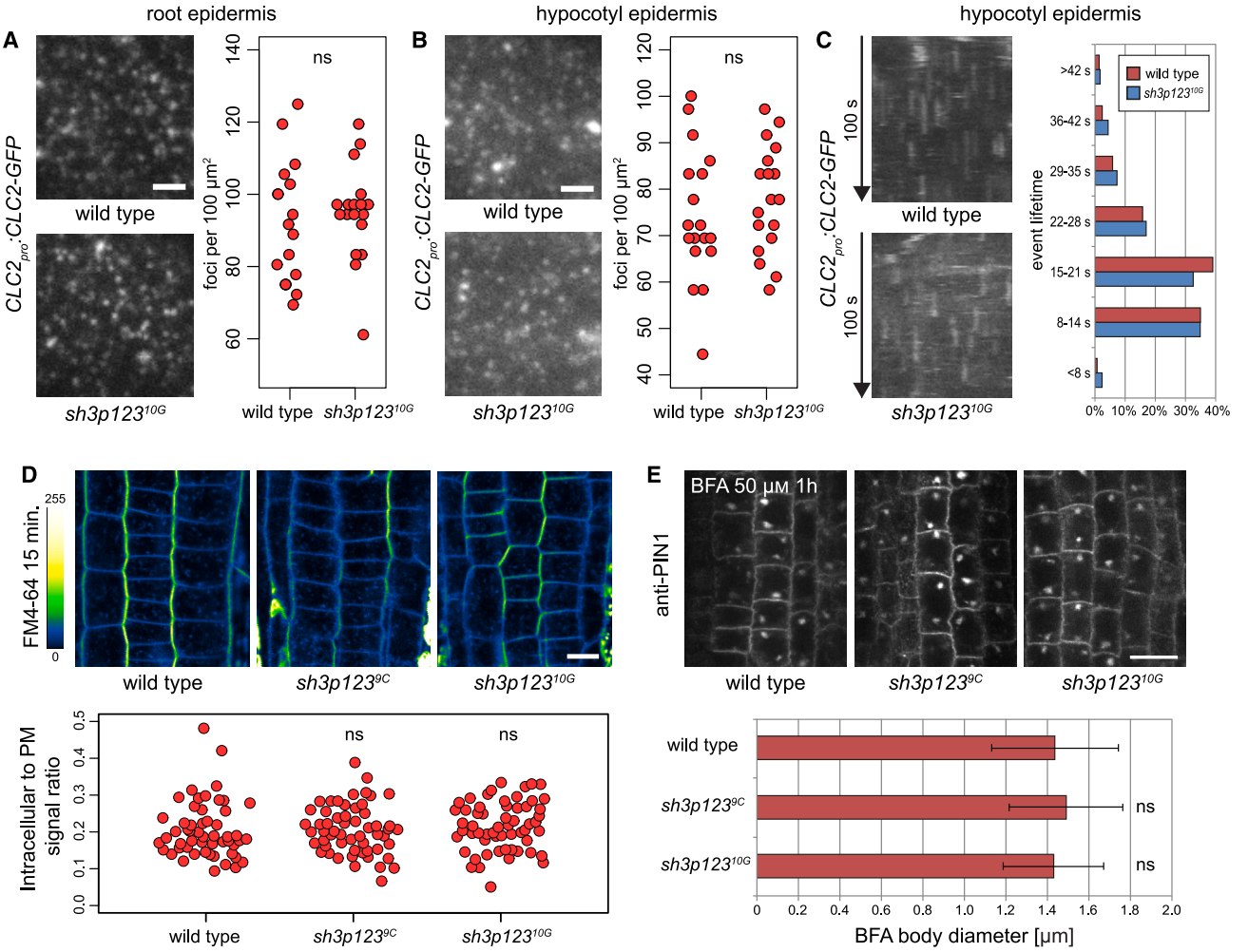

Figure 2. Evaluation of CME in *sh3p123*

(A) TIRF images of CLC2-GFP in the epidermis of early elongation zone of seedling roots of the wild type and *sh3p123*^{10G}. Scale bar, 2 µm. The graph shows quantifications of CLC2-GFP-positive focus density, with each data point representing one root. Wild type: 91.4 ± 16.7 foci per 100 µm^2 (mean ± SD), n = 18; *sh3p123*^{10G}: 94.9 ± 13.1 foci per 100 µm^2, n = 18. Values were compared using a t test. ns, not significant.

(B) TIRF images of CLC2-GFP in the hypocotyl epidermis of the wild type and *sh3p123*^{10G}. Scale bar, 2 µm. The graph shows quantifications of CLC2-GFP-positive focus density, with each data point representing one cell. Wild type: 74.2 ± 14.2 foci per 100 µm^2 (mean ± SD), n = 18; *sh3p123*^{10G}: 77.9 ± 11.5 foci per 100 µm^2, n = 18. Values were compared using a t test.

(C) Kymographs from TIRF videos representing the dynamics of CLC2-GFP in the hypocotyl epidermis of the wild type and *sh3p123*^{10G}. The histogram shows the distribution of lifetimes of single endocytic events at the PM. Wild type, n = 292; *sh3p123*^{10G}, n = 301.

(D) FM4-64 uptake into RAM epidermis of the wild type, *sh3p123*^{9C}, and *sh3p123*^{10G}. Scale bar, 10 µm. The graph shows quantifications of intracellular to PM signal ratios, with each data point representing one root. Wild type: 0.21 ± 0.08 (mean ± SD), n = 53; *sh3p123*^{9C}: 0.21 ± 0.07, n = 56; *sh3p123*^{10G}: 0.22 ± 0.07, n = 58. Mutant values were compared with the wild type using t tests.

(E) Immunostaining of PIN1 in RAM stele after a BFA treatment in the wild type, *sh3p123*^{9C}, and *sh3p123*^{10G}. Scale bar, 10 µm. The graph shows quantifications of BFA body diameters from a representative experiment. Wild type: 1.44 ± 0.31 µm (mean ± SD), n = 170; *sh3p123*^{9C}: 1.49 ± 0.27, n = 120; *sh3p123*^{10G}: 1.43 ± 0.24, n = 120. Mutant values were compared to the wild type using t tests.

Mock treatment is shown in Figure S4.

SH3P1–SH3P3 associate with AUXILIN-LIKE1/2 at the PM

In non-plant systems, endophilin and amphiphysin interact at CCPs with Pro-rich domain-containing partners, synaptojanin and dynamin.[10–12] Protein-protein interactions support the notion that SH3Ps engage with the putative uncoating factors AUXILIN-LIKE1/2,[18,22,24] possibly to recruit them to CCPs. In TIRF imaging studies, AUXILIN-LIKE1 was observed binding to a subset of CCPs at late stages of formation.[24] Additionally, AUXILIN-LIKE1 associated with the PM at sites not containing clathrin. Overall, the localization pattern and dynamics of AUXILIN-LIKE1 at the PM are very similar to those of SH3P2.

To test whether SH3P2 and AUXILIN-LIKE1 localize at the PM together, indicative of physical and functional associations

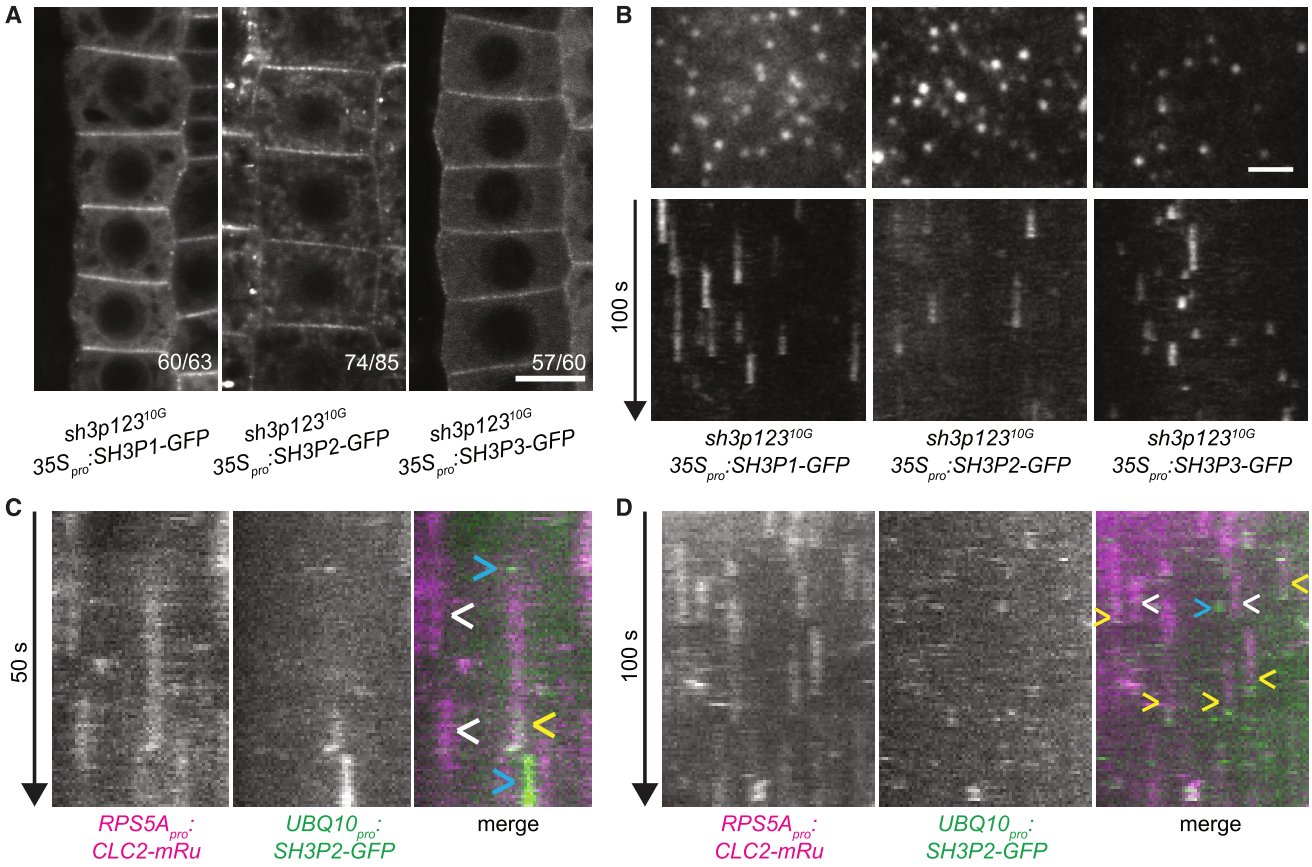

Figure 3. PM localization of SH3P1–SH3P3 and recruitment to CCPs

(A) CLSM images of SH3P1-GFP, SH3P2-GFP, and SH3P3-GFP in RAM epidermis of complemented *sh3p123*^{10G} mutants. All fluorescent protein fusions are enriched at the PMs, while SH3P2-GFP additionally localizes to intracellular structures. Numbers show frequencies of the presented localization pattern. Scale bar, 10 μm. See also Figure S5.

(B) Single TIRF frames (top) and kymographs (bottom) of TIRF time-lapses of SH3P1-GFP, SH3P2-GFP, and SH3P3-GFP in the epidermis of the early elongation zone of seedling roots in complemented *sh3p123*^{10G} mutants. All fluorescent protein fusions localize to the PM as distinct foci, which persist for varied amounts of time. Scale bar,2 μm. See also Figure S6A.

(C and D) Kymographs of TIRF time-lapse colocalization between CLC2-mRuby3 and SH3P2-GFP in the epidermis of the root early elongation zone (C) and of etiolated hypocotyls (D). SH3P2-GFP is recruited at the end of some instances of CCV formation (yellow arrowheads). In (C), the completed CCV with SH3P2-GFP can be seen departing from the PM to the left in the plane of section before the signal disappears, presumably due to vesicle uncoating. Many captured CCPs do not recruit SH3P2-GFP (white arrowheads). SH3P2-GFP is also recruited at sites not containing clathrin (blue arrowheads).
See also Figure S6B.

between the functionally redundant SH3P1–SH3P3 and AUXILIN-LIKE1/2, we generated a double marker line, *UBQ10*$_{pro}$*:SH3P2-GFP UBQ10*$_{pro}$*:mCherry-AUXILIN-LIKE1*. In TIRF microscopy time-lapses, the two fluorescent markers revealed a striking degree of co-localization, where, in most instances, they arrived at the PM and left it simultaneously at the same locations (Figure 4A, yellow arrowheads). Some instances of SH3P2-GFP recruitment without associated mCherry-AUXILIN-LIKE1 could be seen as well (Figure 4A, blue arrowheads). The high degree of spatiotemporal co-localization strongly indicates that SH3P1–SH3P3 interact with AUXILIN-LIKE1/2 at the PM. Given that a fraction of both these proteins is found at sites distinct from clathrin (Figures 3C and 3D),[24] many of these interactions may not take place at CCPs, but it is likely that common recruitment and interactions between SH3P1–SH3P3 and AUXILIN-LIKE1/2 occur at CCPs as well.

The most likely scenario linking SH3P1–SH3P3 and AUXILIN-LIKE1/2 at the PM is direct membrane binding of SH3P1–SH3P3 through BAR domains and recruitment of AUXILIN-LIKE1/2 by Pro-rich-SH3 domain interaction. Therefore, we tested whether SH3P1–SH3P3 are required for AUXILIN-LIKE1/2 localization at the PM by imaging mCherry-AUXILIN-LIKE1 in the *sh3p123*^{10G} background. When assessed with CLSM in seedling RAM epidermis, the PM-associated signals of mCherry-AUXILIN-LIKE1 were virtually lost in the mutant (Figure 4B), and a major portion of the protein was instead present in the cytosol. The relative mCherry-AUXILIN-LIKE1 signal intensity at the PM was not correlated with absolute expression levels in individual seedlings (Figure 4B). This experiment confirmed the notion that the PM recruitment of AUXILIN-LIKE1/2 is mediated by SH3P1–SH3P3.

We analyzed this in further detail by co-localizing mCherry-AUXILIN-LIKE1 with CLC2-GFP in *sh3p123*^{10G} by TIRF microscopy to

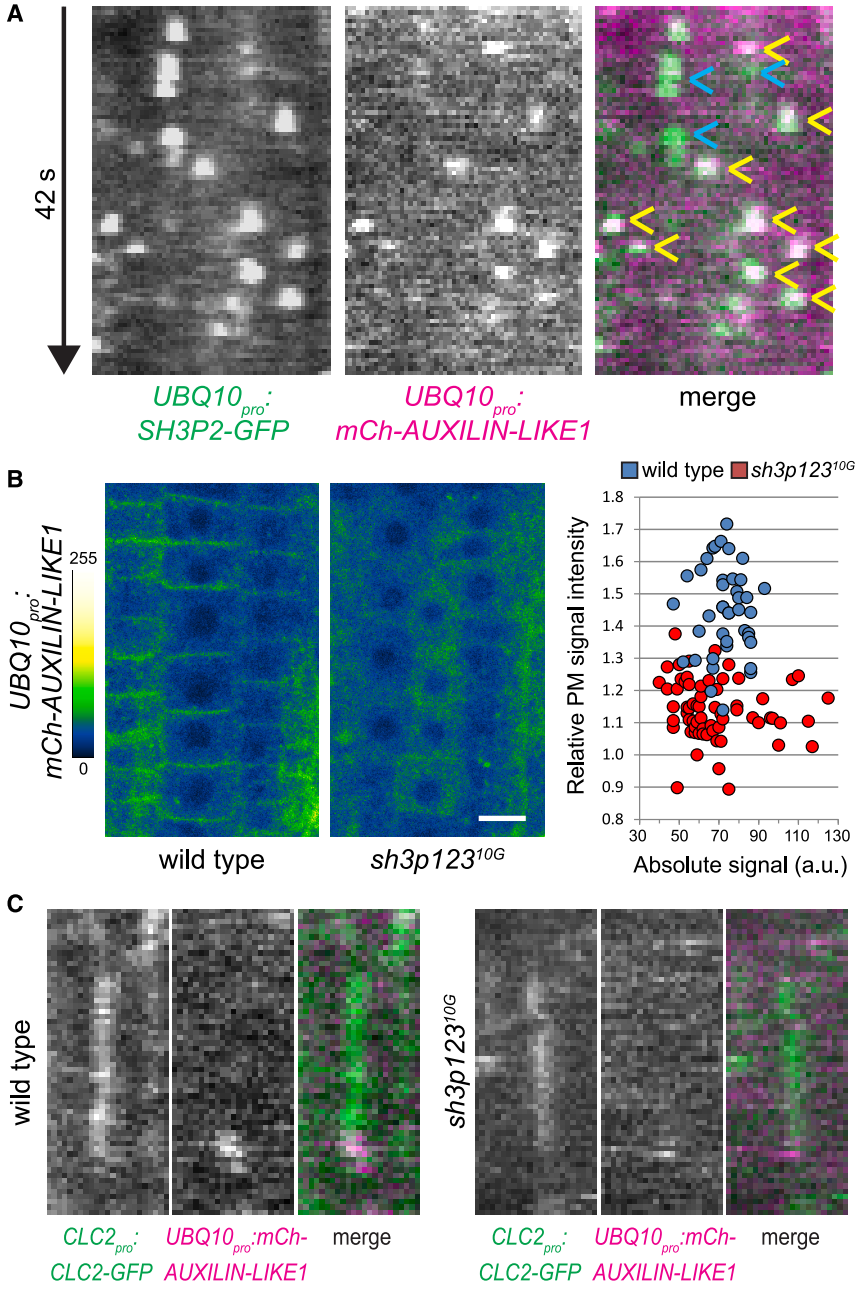

Figure 4. SH3P1–SH3P3 recruit AUXILIN-LIKE1/2 to the PM

(A) Kymographs of TIRF time-lapse colocalization between SH3P2-GFP and mCherry-AUXILIN-LIKE1 in the epidermis of etiolated hypocotyls. The two fluorescent protein fusions exhibit a high degree of colocalization at structures of typically brief lifetimes (yellow arrowheads). SH3P2-GFP is also recruited at sites not containing mCherry-AUXILIN-LIKE1 (blue arrowheads).

(B) CLSM images of mCherry-AUXILIN-LIKE1 in wild-type and *sh3p123* seedling RAM epidermis. The localization of mCherry-AUXILIN-LIKE1 to the PM is almost completely lost in the mutant. Scale bar, 10 μm. The graph shows PM signal intensities relative to total signals in individual seedlings and the distribution of absolute signal levels. Relative PM signal intensities: wild type 1.45 ± 0.14 (mean ± SD), $n = 41$, *sh3p123* 1.14 ± 0.09, $n = 65$. Values were compares using a t test; $p < 0.0001$.

(C) Kymographs of TIRF time-lapse colocalization between CLC2-GFP and mCherry-AUXILIN-LIKE1 in the epidermis of etiolated hypocotyls of the wild type and *sh3p123*. Events of recruitment of mCherry-AUXILIN-LIKE1 at the end of CCV formation can be observed in both genotypes.

See also Figure S6C.

verify specifically whether events of AUXILIN-LIKE1 recruitment at the conclusion of CCV formation occur in the absence of SH3P1–SH3P3. While a quantitative comparison between genotypes was not feasible due to the rarity of reliable detection of these events,[24] some such co-localizations could be decisively observed in the mutant, just like in the wild type (Figures 4C and S6C), indicating that AUXILIN-LIKE1 activity at forming CCVs is possible, at least to some degree, also in the absence of SH3P1–SH3P3.

Putting all the observations together, we conclude that SH3P1–SH3P3 clearly possess a function in the PM recruitment of AUXILIN-LIKE1/2, but an additional mechanism of their recruitment to CCPs likely operates as well.

Distinct responses of SH3P2 to clathrin silencing and AUXILIN-LIKE1 overexpression

Overexpression of AUXILIN-LIKE1/2, or silencing *CHC* with amiRNA, leads to inhibition of CME.[24,35] In both cases, interference with CME manifests similarly in terms of the endocytic machinery. In each case, the recruitment of CLC2-GFP to CCPs is diminished, while subunits of early acting TPC and AP-2 (ADAPTOR PROTEIN 2)[36] remain at the PM and exhibit elevated binding, indicating that inhibition of CME occurred after the initial adaptor binding and at the stage of clathrin recruitment. In both cases, too, the dynamin DRP1C-GFP shows a partial, variable signal decrease.[24,35]

We tested how SH3P2-GFP responds to the inhibition of CME in these two lines. Silencing of *CHC* in *XVE»amiCHCa* led to loss of SH3P2-GFP from the PM in almost all seedlings analyzed by CLSM (Figure 5A). Similarly, TIRF in the early elongation zone of the root showed loss of most of the punctate PM signals, and SH3P2-GFP was found preferentially in the cytosol (Figure 5C, center). This is consistent with a function of SH3P1–SH3P3 as late-acting components of CCPs

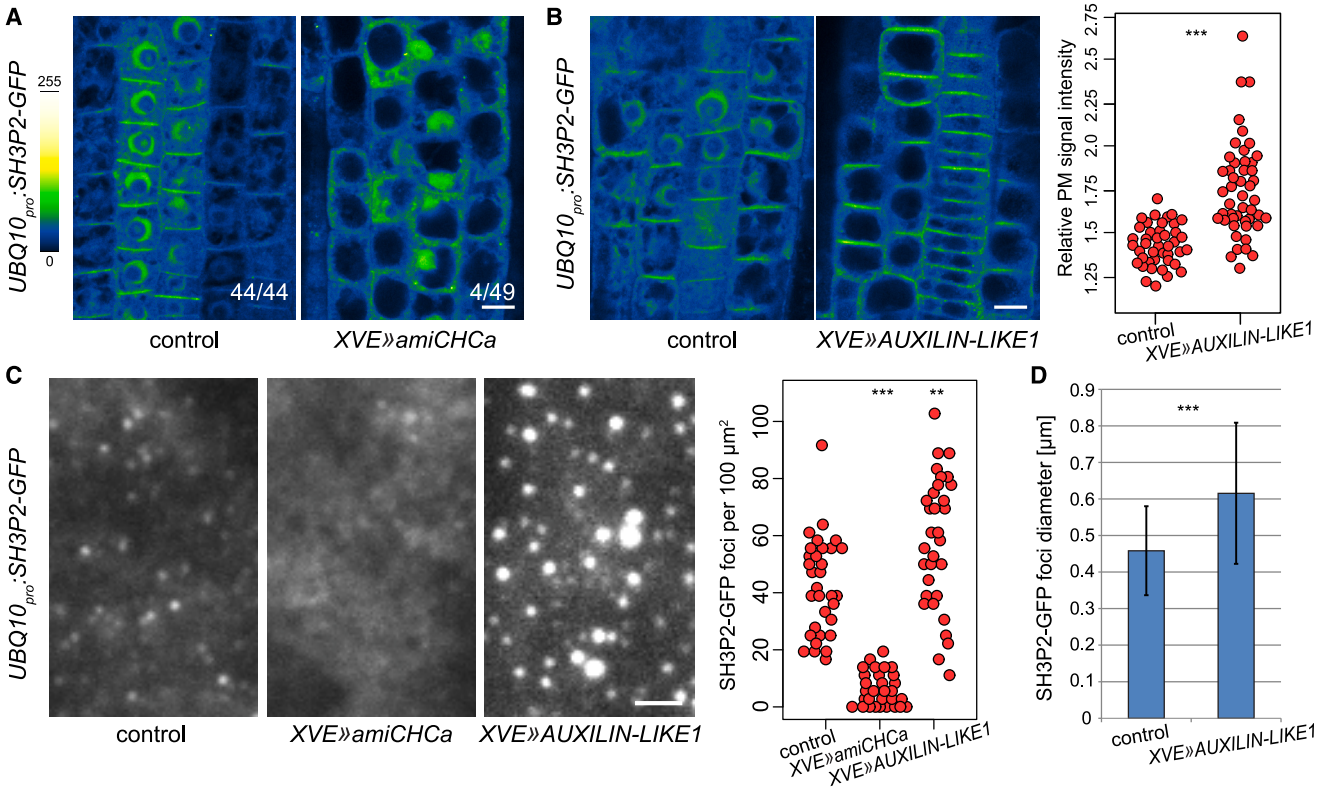

Figure 5. A distinct reaction of SH3P2-GFP to AUXILIN-LIKE1 overexpression compared with clathrin silencing

(A) CLSM images of SH3P2-GFP in seedling RAM epidermis of *XVE»amiCHCa* induced for approximately 48 h and control. Silencing of *CHC* leads to a loss of SH3P2-GFP signals from the PM. Numbers indicate frequencies of RAMs with PM signals of SH3P2-GFP. Scale bar, 10 µm.

(B) CLSM images of SH3P2-GFP in seedling RAM epidermis of *XVE»AUXILIN-LIKE1* induced for approximately 24 h and control. Overexpression of AUXILIN-LIKE1 leads to increases in the PM signal relative to total RAM signals. Scale bar, 10 µm. The graph shows a quantification of relative PM signal intensities, with each data point representing one root. Control: 1.43 ± 0.12 (mean ± SD), $n = 42$; *XVE»AUXILIN-LIKE1:* 1.75 ± 0.27, $n = 48$. Values were compared using a t test; $p < 0.0001$.

(C) TIRF images of SH3P2-GFP in seedling root epidermis of controls as well as *XVE»amiCHCa* and *XVE»AUXILIN-LIKE1* induced for approximately 48 h and 24 h, respectively. Following *CHC* silencing, SH3P2-GFP is observed as cytosolic background with only rare clear foci of signal. Overexpression of AUXILIN-LIKE1 causes an accumulation of SH3P2-GFP signal in abundant foci, which are often enlarged. Scale bar, 2 µm. Graph shows a quantification of SH3P2-GFP focus densities, with each data point representing one cell. Control: 42.3 ± 16.9 foci per 100 µm² (mean ± SD), $n = 32$; *XVE»amiCHCa:* 6.2 ± 5.9 foci per 100 µm², $n = 30$; *XVE»AUXILIN-LIKE1*: 57.7 ± 23.1 foci per 100 µm², $n = 32$. Mutant line values were compared with the control using t tests; ***$p < 0.0001$, **$p = 0.0034$.

(D) Quantification of SH3P2-GFP focus diameters in control and *XVE»AUXILIN-LIKE1* induced for approximately 24 h. Control: 0.46 ± 0.12 µm (mean ± SD), $n = 175$; *XVE»AUXILIN-LIKE1*: 0.62 ± 0.19 µm, $n = 199$. Values were compared using a t test; $p < 0.0001$.

and, as such, not engaging in vesicle formation events arrested at early stages. Given that SH3P2-GFP is often present at the PM at sites not containing clathrin, this recruitment may have been abolished in *XVE»amiCHCa* as well, for unknown reasons.

Interestingly, the response of SH3P2-GFP to AUXILIN-LIKE1 overexpression was different: CLSM revealed that SH3P2-GFP not only remained at the PM, but the relative PM binding levels were higher than under control conditions (Figure 5B). Consistently, TIRF showed abundant, often enlarged foci of SH3P2-GFP signal (Figures 5C, right, 5D). This unexpected reaction of SH3P2-GFP to AUXILIN-LIKE1 overexpression, distinct from the effect of clathrin silencing, constitutes a further indication of a functional tie between SH3P1–SH3P3 and AUXILIN-LIKE1/2.

SH3P1–SH3P3 and TPC are functionally redundant in CME but not due to a shared activity of their SH3 domains

Our analysis of SH3P1–SH3P3 indicates their activity at CCPs, including in the recruitment of AUXILIN-LIKE1/2. Yet, the deleterious consequences of *sh3p123* loss of function are relatively mild (Figure 1) and not associated with a detectable deficiency in CME as a whole (Figure 2). We speculated about a possible functional redundancy between SH3P1–SH3P3 and another, unknown component. One of the two other proteins with predicted SH3 domains in *A. thaliana* is the TPC subunit TASH3 (TPLATE ASSOCIATED SH3 DOMAIN-CONTAINING PROTEIN).[36,37] TPC, belonging to the TSET complex class, is structurally homologous to the tetrameric adaptor protein complexes AP-1 through AP-5, some of which act as clathrin adaptors.[38] TASH3 is, in this

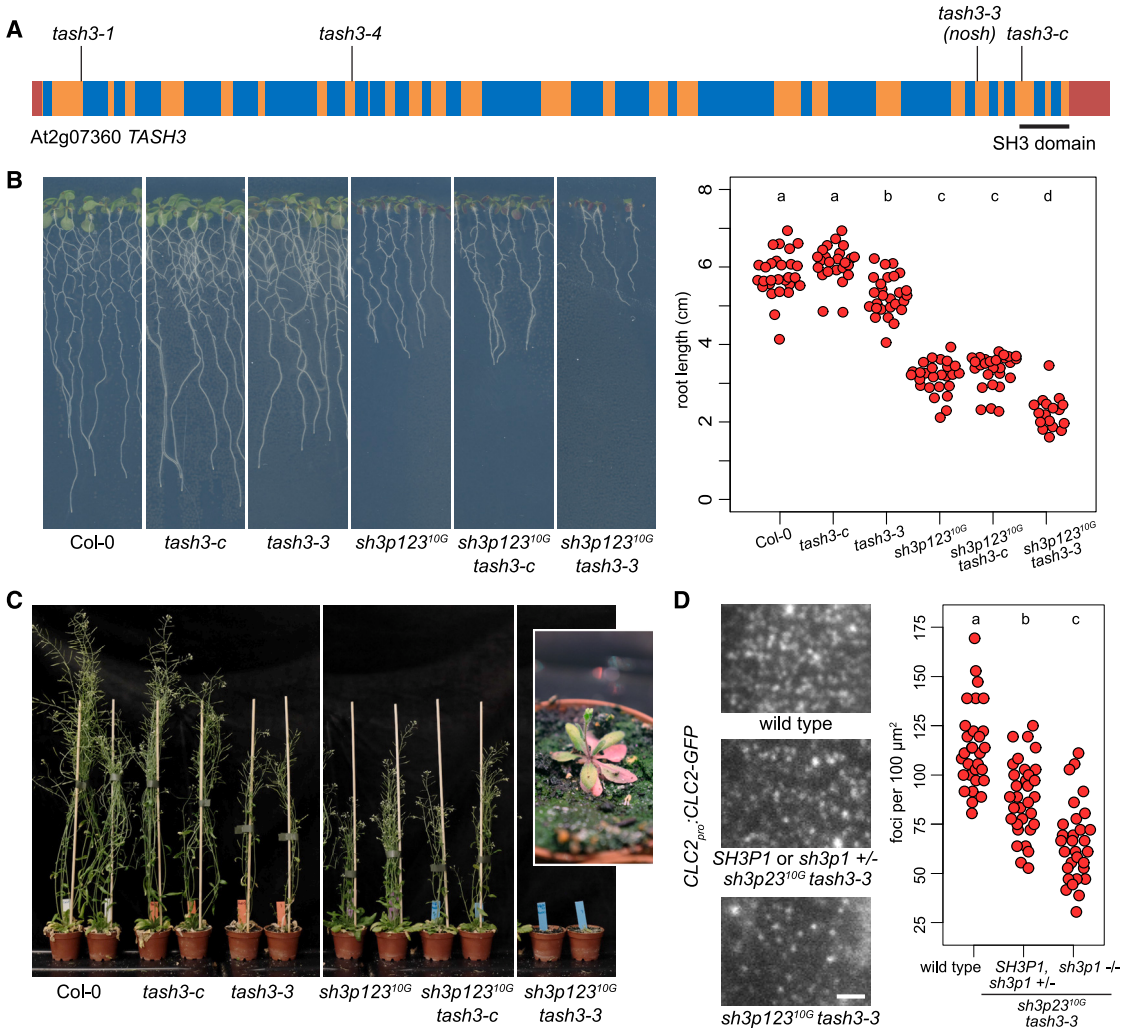

Figure 6. Connections between SH3P1–SH3P3 and TASH3 function

(A) *TASH3* gene structure and mutant alleles. Exons are represented in orange, introns in blue, and UTRs in red. The sequence encoding the C-terminal SH3 domain is underlined. Insertion sites of the T-DNA alleles *tash3-1, tash3-4* and *tash3-3 (nosh)*, as well as the site of the CRISPR-Cas9-induced mutation in *tash3-c*, are indicated. See also Figure S7.

(B) Seedlings of *tash3-c* and *tash3-3* single mutants and in combination with *sh3p123*^{10G}. For clarity, the rightmost panel shows *sh3p123*^{10G} *tash3-3* quadruple homozygotes after the removal of lower-order mutant seedlings from a population segregating for *sh3p1*. The graph shows main root lengths of individual seedlings after 9 days of *in vitro* growth from a representative experiment (3 replicates). Col-0: 5.80 ± 0.58 cm (mean ± SD), $n = 28$; *tash3-c*: 6.08 ± 0.49 cm, $n = 24$; *tash3-3*: 5.26 ± 0.51 cm, $n = 27$; *sh3p123*^{10G}: 3.16 ± 0.41 cm, $n = 26$; *sh3p123*^{10G} *tash3-c*: 3.33 ± 0.44 cm, $n = 27$; *sh3p123*^{10G} *tash3-3*: 2.24 ± 0.43 cm, $n = 17$. Values were compared using one-way ANOVA ($p < 0.00001$) with post hoc Tukey Honest Significant Difference (HSD) test; groups of significantly different values are indicated.

(C) Adults of *tash3-c* and *tash3-3* single mutants and in combination with *sh3p123*^{10G}. Inset: a magnified view of *sh3p123*^{10G} *tash3-3*.

(D) TIRF images of CLC2-GFP in the epidermis of the early elongation zone of seedling roots of the wild type, *sh3p123*^{10G} *tash3-3*, and lower-order mutants in a population segregating for *sh3p1*. Scale bar, 2 µm. The graph shows a quantification of CLC2-GFP focus density, where each data point represents one root. Wild type: 113.9 ± 21.0 foci per 100 µm^2 (mean ± SD), $n = 30$; *SH3P1* and *sh3p1*$^{+/-}$ *sh3p23*$^{-/-}$ *tash3-3*$^{-/-}$: 88.4 ± 18.9 foci per 100 µm^2, $n = 32$; *sh3p123*^{10G} *tash3-3*: 65.6 ± 19.8 foci per 100 µm^2, $n = 30$. Values were compared using one-way ANOVA ($p < 0.00001$) with post hoc Tukey HSD test; groups of significantly different values are indicated.

context, a homolog of the γαδεζ large subunit of APs but uniquely contains an SH3 domain at the C terminus, absent not only in AP complexes but also in non-plant TSET.[37,39] The SH3 domain-containing appendage of TASH3 is required for the recognition of ubiquitinated cargo by TPC.[37]

To assess whether the SH3 domain of TASH3 functionally overlaps with those of SH3P1–SH3P3, we isolated *tash3* mutants and introduced them into *sh3p123*. Mutants of TPC subunits exhibit male gametophytic lethality, precluding a straightforward loss-of-function analysis.[36] Indeed, we could not recover homozygotes of *tash3-1* and *tash3-4* lines harboring T-DNA insertions in early exons of *TASH3* (Figure 6A), presumably due to lethality of mutant male gametes. Instead, given that the SH3 domain of TASH3 is C terminal, we attempted to isolate mutants where

only the sequence coding for the SH3 domain is disrupted. This may lead to the expression of a truncated but functional TASH3 protein containing all parts of structure homologous to subunits of AP complexes. We obtained mutants of this kind by two approaches. First, we isolated *tash3-3,* an exon T-DNA insertion shortly before the sequence encoding the SH3 domain (Figure 6A), known also as *nosh*.[37] Conceptual translation based on re-sequencing of the T-DNA border predicted a TASH3 protein terminated before the SH3 domain (Figure S7A). Additionally, we targeted the SH3 domain by CRISPR-Cas9, generating a *tash3-c* allele with a single-nucleotide insertion early in the SH3 domain-encoding sequence, leading to a stop codon within this domain in the predicted protein (Figures 6A and S7A).

In contrast with *tash3-1* and *tash3-4*, both *tash3-3* and *tash3-c* were viable as homozygotes but, surprisingly, exhibited distinct phenotypes. While *tash3-c* was indistinguishable from the wild type during seedling and adult development (Figures 6B and 5C), *tash3-3* had slightly reduced seedling root lengths (Figure 6B) and clearly deficient adult development, with a reduced number of stems and early senescence of rosette leaves (Figure 6C). Since both alleles delete the SH3 domain, the phenotype exhibited by *tash3-3* indicates additional effects of the T-DNA insertion, possibly reduced gene expression. We tested *TASH3* expression levels in *tash3-3 and tash3-c* by qPCR and found that both alleles had reduced transcript levels, but the expression in *tash3-3* was lower than in *tash3-c* across biological replicates and experiment repetitions (Figure S7B). It might be that *TASH3* transcript levels explain the phenotypic difference between mutant alleles, but additional effects on translation from the abnormal *tash3-3* mRNA, presumably containing parts of the T-DNA sequence, or effects on tash3-3 protein stability or the ability to form protein complexes,[37] may contribute. Overall, the normal phenotype of *tash3-c* suggests that the SH3 domain of TASH3 has no evidently detectable, non-redundant function. By comparison, in our view, the *tash3-3* phenotype cannot be explained by the loss of the SH3 domain alone, and we interpret it here as a partial loss of function of TASH3 as a whole and, by extension, presumably as a partial loss of function of TPC, in which TASH3 is a core component.

We introduced both *tash3-3* and *tash3-c* into *sh3p123*^{10G} to assess genetic interactions. A potential redundant function of the SH3 domains of TASH3 and SH3P1–SH3P3 could be tested in *sh3p123*^{10G} *tash3-c*. This quadruple homozygote exhibited phenotypes identical to *sh3p123*^{10G} both at seedling and adult stages of development (Figures 6B and 6C), indicating that the SH3 domain of TASH3 does not contribute to a function redundant with SH3P1–SH3P3. In turn, *sh3p123*^{10G} *tash3-3* was, in our view, informative about a functional relationship between SH3P1–SH3P3 and TPC in a more general sense. These quadruple mutants had diminished seedling root growth rates in comparison to both parental lines (Figure 6B), while as adults, they exhibited a striking phenotype characterized by the development of very small plants with reduced rosette leaves, rarely bolting, and producing only up to a few flowers on short inflorescence stems (Figure 6C). These plants were infertile, and the line was maintained as an *sh3p1* heterozygote.

Exploring this further, we assessed rates of CME in *sh3p123*^{10G} *tash3-3* using the clathrin marker CLC2-GFP and TIRF microscopy in the early elongation zones of seedling roots. Segregating plants wild type or heterozygous for *sh3p1* had a relatively mild decrease in CCP density compared with the wild type (Figure 6D). This decrease is typical for *tash3-3* alone, as similar observations were made with several other markers of CME in the single mutant.[37,40] In turn, *sh3p123*^{10G} *tash3-3* quadruple homozygotes had a strongly decreased density of CCPs at the PM (Figure 6D). This finding demonstrates a contribution of SH3P1–SH3P3 to the overall cellular endocytic activity, which was not detected when SH3P1–SH3P3 function alone was abolished (Figure 2) but which manifested in a sensitized genetic background.

Taken together, we did not find evidence for a common function of the SH3 domains of TASH3 and SH3P1–SH3P3, as shown by the lack of effects of the *tash3-c* allele, where the SH3 domain of TASH3 is abolished with a relative specificity. In comparison, *tash3-3,* interpreted as a partial loss of function of TPC, revealed a role of SH3P1–SH3P3 in CME, masked in the original mutant, and manifested by strong deficiencies in overall growth and development, as well as in CCP formation, in the mutant cross.

DISCUSSION

SH3P1–SH3P3 as endophilin/amphiphysin homologs engaged in an interaction with auxilin-likes

Here, we characterize the BAR-SH3 domain proteins SH3P1–SH3P3 of *A. thaliana* as homologs of endophilin and amphiphysin, which play important roles at late stages of CME in non-plant systems.[13,16] SH3P1–SH3P3 dynamically localize to discrete foci at the PM, and colocalization indicates specific recruitment at the late stage of CCP formation in a subset of CME events, similarly to non-plant counterparts.[7] Previously reported protein-protein interactions between specific SH3P and AUXILIN-LIKE isoforms detected with yeast two hybrid assay, coimmunoprecipitation, tandem affinity purification, and bimolecular fluorescence complementation;[18,22,24] the remarkable level of spatiotemporal colocalization of SH3P2 and AUXILIN-LIKE1 at the PM; and the reaction of SH3P2-GFP to AUXILIN-LIKE1 overexpression all indicate that SH3P1–SH3P3 function at the PM is associated with the presumed auxilin-like uncoating factors AUXILIN-LIKE1/2. SH3P1–SH3P3 promote AUXILIN-LIKE1/2 localization at the PM, likely including the late recruitment at CCPs, as seen by the loss of AUXILIN-LIKE1 from the PMs in *sh3p123*. Yet, parallel mechanisms may contribute to AUXILIN-LIKE1/2 recruitment to CCPs, since some events of such recruitment could still be detected in *sh3p123*. Taken as a whole, our findings provide strong support for a plant-specific interaction module in CME, where BAR-SH3 domain-containing proteins engage with auxilin-likes, most likely to promote vesicle uncoating. While we postulate that this function is shared between the three isoforms, the additional intracellular localization of SH3P2, but not SH3P1 or SH3P3, suggests that other activities of SH3P2 may be unique to this relatively better characterized isoform.[22,26–28]

Additional functions of SH3P1–SH3P3 in endocytosis

In many instances, uncoating of CCVs in plants may not take place immediately at vesicle departure from the PM but be

delayed, as endocytic vesicles with coats can be observed arriving at the early endosome compartment.[2] Uncoating of such vesicles at or on the way toward the early endosome may involve the SAC9 phosphoinositide phosphatase.[22] Interestingly, SAC9 physically interacts with SH3P2, and SH3P2 localization at the PM depends on SAC9.[22] It remains to be fully elucidated how SH3Ps may be involved in a synaptojanin-like uncoating mechanism in plants.

When considering other endocytic functions of SH3P1–SH3P3, notable are the previously reported interactions of SH3P1–SH3P3 with dynamins, analogical to the mechanism of action of endophilin and amphiphysin in non-plant models. SH3P1 and SH3P2 have been reported to interact with DYNAMIN-RELATED PROTEIN 1A (DRP1A),[20,21] possibly indirectly, given that DRP1A does not possess Pro-rich regions. In turn, SH3P2 and SH3P3 interact with DRP2A, which, like its homolog DRP2B, contains Pro-rich domains.[19,41] Despite this, a recent analysis indicates that the recruitment of DRP2 dynamins to CCVs is not dependent on SH3Ps, suggestive of an unknown, plant-specific mechanism supporting vesicle scission.[41]

Finally, it may be speculated that SH3P1–SH3P3 participate in a clathrin-independent mode of endocytosis, similarly to endophilin, which acts in a pathway known as fast endophilin-mediated endocytosis.[42] Localization of SH3P2-GFP to foci at the PM not containing clathrin is supportive of this possibility, but the likely presence of AUXILIN-LIKE1 there, and the apparent sensitivity of all PM localization of SH3P2-GFP to clathrin silencing, are not fully consistent with this scenario.

Implications of the genetic interaction with TPC

Quantitatively, the function of SH3P1–SH3P3 in CME was best revealed in a genetic interaction between *sh3p123* and *tash3-3/nosh*.[37] We interpret *tash3-3* as a partial loss of function of TPC, rather than specifically affecting the SH3 domain of its subunit TASH3, through a comparison with *tash3-c*, where a deletion of this SH3 domain did not lead to evident deleterious effects. Alternatively, the phenotype of *tash3-3* may result from the loss of the linker sequence before the SH3 domain, which is retained in *tash3-c* (Figure S7A). Regardless of this, the strong deficiencies in CME in *sh3p123 tash3-3* allowed us to demonstrate a contribution of SH3P1–SH3P3 to this process, but the observations also lead to questions regarding the distinct possible courses that CCV formation can take. The discussed genetic analysis indicates that CME can function well without SH3P1–SH3P3, but only if TPC is fully active *(sh3p123 TASH3)*, or with only partial TPC function, provided that SH3P1–SH3P3 are present instead *(SH3P tash3-3)*, but not if both are lost simultaneously. In which sense are SH3P1–SH3P3 redundant with TPC, if the latter acts in vesicle formation from the early stages, as an adaptor[36] or in membrane bending,[43] while SH3P1–SH3P3 are recruited to CCPs late, contributing to uncoating? If TPC and SH3P1–SH3P3 contribute to vesicle formation redundantly but by distinct molecular activities, then a situation emerges where CME may proceed effectively through distinct molecular mechanisms provided by coats of distinct compositions rather than resembling a linear pathway of obligatory components. This and similar examples of genetic interactions in CME[40] suggest that such flexibility of the endocytic process is a likely scenario.

Limitations of the study

We recognize two main limitations of this study. First, while PM recruitment of AUXILIN-LIKE1 depends on SH3P1–SH3P3, we were unable to evaluate quantitatively whether the late recruitment of AUXILIN-LIKE1 to CCPs is reduced specifically in the absence of SH3P1–SH3P3. Second, while several lines of evidence indicate that AUXILIN-LIKE1/2 are uncoating factors similar to non-plant auxilins,[24] there is, at present, only limited direct evidence for this biochemical activity.[18]

STAR★METHODS

Detailed methods are provided in the online version of this paper and include the following:

- KEY RESOURCES TABLE
- RESOURCE AVAILABILITY
  - Lead contact
  - Materials availability
  - Data and code availability
- EXPERIMENTAL MODEL AND STUDY PARTICIPANT DETAILS
- METHOD DETAILS
  - Confocal laser scanning microscopy
  - FM4-64 staining
  - PIN1 immunolocalization
  - Total Internal Reflection Fluorescence microscopy
  - Molecular cloning
  - CRISPR/Cas9 mutagenesis
  - Quantitative reverse transcriptase PCR
  - Accession numbers
- QUANTIFICATION AND STATISTICAL ANALYSIS

SUPPLEMENTAL INFORMATION

Supplemental information can be found online at https://doi.org/10.1016/j.celrep.2024.114195.

ACKNOWLEDGMENTS

The authors wish to acknowledge Dr. Daniel van Damme for mRuby3/pDONRP2rP3 and Prof. Qi-Jun Chen for sharing plasmids used for CRISPR-Cas9 mutagenesis. This work was supported by the Austrian Science Fund (FWF): I 3630-B25.

AUTHOR CONTRIBUTIONS

M.A. and J.F. designed the research, analyzed data, and wrote the manuscript. M.A., M.R., and I.M. performed the research. M.N. generated *RPS5A:CLC2-mRuby*.

DECLARATION OF INTERESTS

The authors declare no competing interests.

Received: October 8, 2023
Revised: March 9, 2024
Accepted: April 19, 2024

REFERENCES

1. Dhonukshe, P., Aniento, F., Hwang, I., Robinson, D.G., Mravec, J., Stierhof, Y.-D., and Friml, J. (2007). Clathrin-Mediated Constitutive Endocytosis of PIN Auxin Efflux Carriers in Arabidopsis. Curr. Biol. *17*, 520–527.

2. Narasimhan, M., Johnson, A., Prizak, R., Kaufmann, W.A., Tan, S., Casillas-Pérez, B., and Friml, J. (2020). Evolutionarily unique mechanistic framework of clathrin-mediated endocytosis in plants. Elife *9*, e52067.
3. Kaksonen, M., and Roux, A. (2018). Mechanisms of clathrin-mediated endocytosis. Nat. Rev. Mol. Cell Biol. *19*, 313–326.
4. Merrifield, C.J., and Kaksonen, M. (2014). Endocytic Accessory Factors and Regulation of Clathrin-Mediated Endocytosis. Cold Spring Harb. Perspect. Biol. *6*, a016733.
5. Nishimura, T., Morone, N., and Suetsugu, S. (2018). Membrane re-modelling by BAR domain superfamily proteins via molecular and non-molecular factors. Biochem. Soc. Trans. *46*, 379–389.
6. Simunovic, M., Evergren, E., Callan-Jones, A., and Bassereau, P. (2019). Curving Cells Inside and Out: Roles of BAR Domain Proteins in Membrane Shaping and Its Cellular Implications. Annu. Rev. Cell Dev. Biol. *35*, 111–129.
7. Taylor, M.J., Perrais, D., and Merrifield, C.J. (2011). A High Precision Survey of the Molecular Dynamics of Mammalian Clathrin-Mediated Endocytosis. PLoS Biol. *9*, e1000604.
8. Carman, P.J., and Dominguez, R. (2018). BAR domain proteins—a linkage between cellular membranes, signaling pathways, and the actin cytoskeleton. Biophys. Rev. *10*, 1587–1604.
9. Kurochkina, N., and Guha, U. (2013). SH3 domains: modules of protein–protein interactions. Biophys. Rev. *5*, 29–39.
10. Ringstad, N., Nemoto, Y., and De Camilli, P. (1997). The SH3p4/Sh3p8/SH3p13 protein family: Binding partners for synaptojanin and dynamin via a Grb2-like Src homology 3 domain. Proc. Natl. Acad. Sci. USA *94*, 8569–8574.
11. Grabs, D., Slepnev, V.I., Songyang, Z., David, C., Lynch, M., Cantley, L.C., and De Camilli, P. (1997). The SH3 Domain of Amphiphysin Binds the Proline-rich Domain of Dynamin at a Single Site That Defines a New SH3 Binding Consensus Sequence. J. Biol. Chem. *272*, 13419–13425.
12. Micheva, K.D., Kay, B.K., and McPherson, P.S. (1997). Synaptojanin Forms Two Separate Complexes in the Nerve Terminal. J. Biol. Chem. *272*, 27239–27245.
13. Shupliakov, O., Löw, P., Grabs, D., Gad, H., Chen, H., David, C., Takei, K., De Camilli, P., and Brodin, L. (1997). Synaptic Vesicle Endocytosis Impaired by Disruption of Dynamin-SH3 Domain Interactions. Science *276*, 259–263.
14. Verstreken, P., Koh, T.-W., Schulze, K.L., Zhai, R.G., Hiesinger, P.R., Zhou, Y., Mehta, S.Q., Cao, Y., Roos, J., and Bellen, H.J. (2003). Synaptojanin Is Recruited by Endophilin to Promote Synaptic Vesicle Uncoating. Neuron *40*, 733–748.
15. Schuske, K.R., Richmond, J.E., Matthies, D.S., Davis, W.S., Runz, S., Rube, D.A., van der Bliek, A.M., and Jorgensen, E.M. (2003). Endophilin Is Required for Synaptic Vesicle Endocytosis by Localizing Synaptojanin. Neuron *40*, 749–762.
16. Milosevic, I., Giovedi, S., Lou, X., Raimondi, A., Collesi, C., Shen, H., Paradise, S., O'Toole, E., Ferguson, S., Cremona, O., and De Camilli, P. (2011). Recruitment of Endophilin to Clathrin-Coated Pit Necks Is Required for Efficient Vesicle Uncoating after Fission. Neuron *72*, 587–601.
17. Reynolds, G.D., Wang, C., Pan, J., and Bednarek, S.Y. (2018). Inroads into Internalization: Five Years of Endocytic Exploration. Plant Physiol. *176*, 208–218.
18. Lam, B.C., Sage, T.L., Bianchi, F., and Blumwald, E. (2001). Role of SH3 Domain-Containing Proteins in Clathrin-Mediated Vesicle Trafficking in Arabidopsis. Plant Cell *13*, 2499–2512.
19. Lam, B.C.-H., Sage, T.L., Bianchi, F., and Blumwald, E. (2002). Regulation of ADL6 activity by its associated molecular network. Plant J. *31*, 565–576.
20. Ahn, G., Kim, H., Kim, D.H., Hanh, H., Yoon, Y., Singaram, I., Wijesinghe, K.J., Johnson, K.A., Zhuang, X., Liang, Z., et al. (2017). SH3 Domain-Containing Protein 2 Plays a Crucial Role at the Step of Membrane Tubulation during Cell Plate Formation. Plant Cell *29*, 1388–1405.
21. Baquero Forero, A., and Cvrčková, F. (2019). SH3Ps—Evolution and Diversity of a Family of Proteins Engaged in Plant Cytokinesis. IJMS *20*, 5623.
22. Lebecq, A., Doumane, M., Fangain, A., Bayle, V., Leong, J.X., Rozier, F., Marques-Bueno, M.D., Armengot, L., Boisseau, R., Simon, M.L., et al. (2022). The Arabidopsis SAC9 enzyme is enriched in a cortical population of early endosomes and restricts PI(4,5)P2 at the plasma membrane. Elife *11*, e73837.
23. Sousa, R., and Lafer, E.M. (2015). The role of molecular chaperones in clathrin mediated vesicular trafficking. Front. Mol. Biosci. *2*, 26.
24. Adamowski, M., Narasimhan, M., Kania, U., Glanc, M., De Jaeger, G., and Friml, J. (2018). A Functional Study of AUXILIN-LIKE1 and 2, Two Putative Clathrin Uncoating Factors in Arabidopsis. Plant Cell *30*, 700–716.
25. Dahhan, D.A., Reynolds, G.D., Cárdenas, J.J., Eeckhout, D., Johnson, A., Yperman, K., Kaufmann, W.A., Vang, N., Yan, X., Hwang, I., et al. (2022). Proteomic characterization of isolated Arabidopsis clathrin-coated vesicles reveals evolutionarily conserved and plant-specific components. Plant Cell *34*, 2150–2173.
26. Nagel, M.-K., Kalinowska, K., Vogel, K., Reynolds, G.D., Wu, Z., Anzenberger, F., Ichikawa, M., Tsutsumi, C., Sato, M.H., Kuster, B., et al. (2017). *Arabidopsis* SH3P2 is an ubiquitin-binding protein that functions together with ESCRT-I and the deubiquitylating enzyme AMSH3. Proc. Natl. Acad. Sci. USA *114*, E7197–E7204.
27. Zhuang, X., Wang, H., Lam, S.K., Gao, C., Wang, X., Cai, Y., and Jiang, L. (2013). A BAR-Domain Protein SH3P2, Which Binds to Phosphatidylinositol 3-Phosphate and ATG8, Regulates Autophagosome Formation in Arabidopsis. Plant Cell *25*, 4596–4615.
28. Leong, J.X., Raffeiner, M., Spinti, D., Langin, G., Franz-Wachtel, M., Guzman, A.R., Kim, J.G., Pandey, P., Minina, A.E., Macek, B., et al. (2022). A bacterial effector counteracts host autophagy by promoting degradation of an autophagy component. EMBO J. *41*, e110352.
29. Aniento, F., and Robinson, D.G. (2005). Testing for endocytosis in plants. Protoplasma *226*, 3–11.
30. Bolte, S., Talbot, C., Boutte, Y., Catrice, O., Read, N.D., and Satiat-Jeunemaitre, B. (2004). FM-dyes as experimental probes for dissecting vesicle trafficking in living plant cells. J. Microsc. *214*, 159–173.
31. Jelínková, A., Malínská, K., Simon, S., Kleine-Vehn, J., Parezová, M., Pejchar, P., Kubeš, M., Martinec, J., Friml, J., Zazímalová, E., and Petrásek, J. (2010). Probing plant membranes with FM dyes: tracking, dragging or blocking? Plant J. *61*, 883–892.
32. Geldner, N., Friml, J., Stierhof, Y.D., Jürgens, G., and Palme, K. (2001). Auxin transport inhibitors block PIN1 cycling and vesicle trafficking. Nature *413*, 425–428.
33. Geldner, N., Anders, N., Wolters, H., Keicher, J., Kornberger, W., Muller, P., Delbarre, A., Ueda, T., Nakano, A., and Jürgens, G. (2003). The Arabidopsis GNOM ARF-GEF mediates endosomal recycling, auxin transport, and auxin-dependent plant growth. Cell *112*, 219–230.
34. Doumane, M., Lebecq, A., Colin, L., Fangain, A., Stevens, F.D., Bareille, J., Hamant, O., Belkhadir, Y., Munnik, T., Jaillais, Y., and Caillaud, M.-C. (2021). Inducible depletion of PI(4,5)P2 by the synthetic iDePP system in Arabidopsis. Nat. Plants *7*, 587–597.
35. Adamowski, M., Matijević, I., and Friml, J. (2021). The role of clathrin in exocytosis and the mutual regulation of endo- and exocytosis in plant cells. bioRxiv. https://doi.org/10.1101/2021.11.17.468992.
36. Gadeyne, A., Sánchez-Rodríguez, C., Vanneste, S., Di Rubbo, S., Zauber, H., Vanneste, K., Van Leene, J., De Winne, N., Eeckhout, D., Persiau, G., et al. (2014). The TPLATE adaptor complex drives clathrin-mediated endocytosis in plants. Cell *156*, 691–704.
37. Grones, P., De Meyer, A., Pleskot, R., Mylle, E., Kraus, M., Vandorpe, M., Yperman, K., Eeckhout, D., Dragwidge, J.M., Jiang, Q., et al. (2022). The endocytic TPLATE complex internalizes ubiquitinated plasma membrane cargo. Nat. Plants *8*, 1467–1483.

38. Sanger, A., Hirst, J., Davies, A.K., and Robinson, M.S. (2019). Adaptor protein complexes and disease at a glance. J. Cell Sci. *132*, jcs222992.

39. Hirst, J., Schlacht, A., Norcott, J.P., Traynor, D., Bloomfield, G., Antrobus, R., Kay, R.R., Dacks, J.B., and Robinson, M.S. (2014). Characterization of TSET, an ancient and widespread membrane trafficking complex. Elife *3*, e02866.

40. Adamowski, M., Matijević, I., and Friml, J. (2022). Characterization of CAP1 and ECA4 adaptors participating in clathrin-mediated endocytosis. bioRxiv. https://doi.org/10.1101/2022.01.07.475412.

41. Gnyliukh, N., Johnson, A., Nagel, M.-K., Monzer, A., Babić, D., Hlavata, A., Alotaibi, S.S., Isono, E., Loose, M., and Friml, J. (2024). Role of dynamin-related proteins 2 and SH3P2 in clathrin-mediated endocytosis in Arabidopsis thaliana. J. Cell Sci. *2024*, jcs.261720. https://doi.org/10.1242/jcs.261720.

42. Casamento, A., and Boucrot, E. (2020). Molecular mechanism of Fast Endophilin-Mediated Endocytosis. Biochem. J. *477*, 2327–2345.

43. Johnson, A., Dahhan, D.A., Gnyliukh, N., Kaufmann, W.A., Zheden, V., Costanzo, T., Mahou, P., Hrtyan, M., Wang, J., Aguilera-Servin, J., et al. (2021). The TPLATE complex mediates membrane bending during plant clathrin–mediated endocytosis. Proc. Natl. Acad. Sci. USA *118*, e2113046118.

44. Konopka, C.A., Backues, S.K., and Bednarek, S.Y. (2008). Dynamics of Arabidopsis Dynamin-Related Protein 1C and a Clathrin Light Chain at the Plasma Membrane. Plant Cell *20*, 1363–1380.

45. Sauer, M., Paciorek, T., Benková, E., and Friml, J. (2006). Immunocytochemical techniques for whole-mount in situ protein localization in plants. Nat. Protoc. *1*, 98–103.

46. Karimi, M., Inzé, D., and Depicker, A. (2002). GATEWAY™ vectors for Agrobacterium-mediated plant transformation. Trends Plant Sci. *7*, 193–195.

47. Wang, Z.-P., Xing, H.-L., Dong, L., Zhang, H.-Y., Han, C.-Y., Wang, X.-C., and Chen, Q.-J. (2015). Egg cell-specific promoter-controlled CRISPR/Cas9 efficiently generates homozygous mutants for multiple target genes in Arabidopsis in a single generation. Genome Biol. *16*, 144.

STAR★METHODS

KEY RESOURCES TABLE

REAGENT or RESOURCE	SOURCE	IDENTIFIER
Experimental models: Organisms/strains		
Arabidopsis thaliana ecotype Col-0	Nottingham Arabidopsis Stock Center (NASC)	N1092
Arabidopsis thaliana sh3p123^{9C}	This study	N/A
Arabidopsis thaliana sh3p123^{10G}	This study	N/A
Arabidopsis thaliana sh3p123^{10G} CLC2$_{pro}$:CLC2-GFP UBQ10$_{pro}$:mCherry-AUXILIN-LIKE1	This study	N/A
Arabidopsis thaliana sh3p1+/−,2,310G tash3-3 CLC2$_{pro}$:CLC2-GFP	This study	N/A
Arabidopsis thaliana tash3-c	This study	N/A
Arabidopsis thaliana UBQ10$_{pro}$:SH3P2-GFP RPS5A$_{pro}$:CLC2-mRuby	This study	N/A
Arabidopsis thaliana UBQ10$_{pro}$:SH3P2-GFP UBQ10$_{pro}$:mCherry-AUXILIN-LIKE1	This study	N/A

RESOURCE AVAILABILITY

Lead contact

Further information and requests for resources should be directed to the lead contact, Jiří Friml (jiri.friml@ist.ac.at).

Materials availability

Requests for lines and constructs generated in this study should be directed to the lead contact.

Data and code availability

- All data reported in this paper will be shared by the lead contact upon request.
- This paper does not report original code.
- Any additional information required to reanalyze the data reported in this work paper is available from the lead contact upon request.

EXPERIMENTAL MODEL AND STUDY PARTICIPANT DETAILS

The study used *A. thaliana* as model. The following previously described *A. thaliana* lines were used in this study: *CLC2$_{pro}$:CLC2-GFP*,[44] *UBQ10$_{pro}$:mCherry-AUXILIN-LIKE1*, *CLC2$_{pro}$:CLC2-GFP UBQ10$_{pro}$:mCherry-AUXILIN-LIKE1*, *XVE»AUXILIN-LIKE1*,[24] *XVE»amiCHCa*,[35] *UBQ10$_{pro}$:SH3P2-GFP*,[27] *sh3p3* (SALK_065970),[26] *tash3-1* +/− (SALKseq_122269), *tash3-3/nosh* (SALK_011079).[37] Lines generated as part of this study with details of mutant alleles are listed in Table S1 and primers used for genotyping in Table S2.

Seedlings were grown in *in vitro* cultures on half-strength Murashige and Skoog (½MS) medium of pH = 5.9 supplemented with 1% (w/v) sucrose and 0.8% (w/v) phytoagar at 21°C in 16h light/8h dark cycles with Philips GreenPower LED as light source, using deep red (660nm)/far red (720nm)/blue (455nm) combination, with a photon density of about 140μmol/(m^{2}s) +/− 20%. β-estradiol (Sigma-Aldrich) was solubilized in 100% ethanol to 5 mg/mL stock concentration and added to ½MS media during preparation of solid media to a final concentration of 2.5 μg/mL. Seedlings of *XVE»AUXILIN-LIKE1* and *XVE»amiCHCa* lines were induced by transferring to β-estradiol-supplemented media at day 3. Petri dishes for TIRF imaging in hypocotyls of etiolated seedlings were initially exposed to light for several hours and then wrapped in aluminum foil.

METHOD DETAILS

Confocal laser scanning microscopy

4 to 5 day old seedlings were used for live imaging with Zeiss LSM800 confocal laser scanning microscope with 20 × 0.8 air and 40 × 1.2 immersion lenses. The *UBQ10$_{pro}$:mCherry-AUXILIN-LIKE1* transgene exhibited silencing, which was particularly visible in the *sh3p123* cross; the experiments were thus conducted on seedlings pre-selected under a fluorescent stereomicroscope as expressing relatively brighter mCherry signals. Images in both genotypes were captured by CLSM with identical detection settings to ascertain validity of the comparison.

FM4-64 staining

Seedlings were stained in liquid ½MS medium with 1% (w/v) sucrose supplemented with 2 μM FM4–64 dye (ThermoFisher) for 5 min, in the dark and on ice. Excess dye was washed out and seedlings mounted in ½MS medium with 1% (w/v) sucrose in microscopy slides at room temperature, marking the start of the internalization time measurement.

PIN1 immunolocalization

Seedlings were incubated in liquid ½MS medium with 1% (w/v) sucrose and containing Brefeldin A (Sigma-Aldrich) at a final concentration of 50 μM or the solvent (DMSO) in controls. Intavis InsituPro VSi robot was used for immunostaining according to the previously published protocol.[45] The following antibodies were used: anti-PIN1, anti-Rabbit-Cy3 (Sigma-Aldrich).

Total Internal Reflection Fluorescence microscopy

Early elongation zone of roots in excised ~1 cm long root tip fragments from 7d old seedlings, as well as apical ends of excised hypocotyls from 3d old etiolated seedlings, were used for TIRF imaging. Imaging was performed with Olympus IX83 TIRF microscope, using a 100X TIRF lens with an additional 1.6X or 2× magnification lens in the optical path. Time lapses of 100 frames at 0.5 s or 1 s intervals with exposure times of 195 ms or 200 ms, or single snapshots of 200 ms exposure, were taken, depending on the experiment. Two-channel time lapses were captured sequentially.

Molecular cloning

All constructs generated in this study are listed in Table S3 and primers used for cloning in Table S2. Sequences of *SH3P1, SH3P3,* and *CLC2* were cloned into pENTR/D-TOPO and pDONR221 entry vectors (Invitrogen). *35S:SH3P1-GFP* and *35S:SH3P3-GFP* were generated in pH7FWG2 expression vectors[46] by LR Clonase II and used for transformation of *sh3p123* alongside the previously cloned 35S:SH3P2-GFP/pH7FWG2.[24] *RPS5A:CLC2-mRuby* was generated in pK7m34GW expression vector[46] by LR Clonase II Plus by combining RPS5A/pDONRP4P1r, CLC2/pDONR221, and mRuby3/pDONRP4P1r.

CRISPR/Cas9 mutagenesis

CRISPR/Cas9 mutagenesis of *SH3P1, SH3P2,* and *TASH3* was performed with the use of pHEE401 binary vector and template plasmids pCBC-DT1T2 and pCBC-DT2T3.[47] sgRNA sequences were selected with the use of CRISPR RGEN Tools website (http://www.rgenome.net/cas-designer/). sgRNA sequences used in each construct are given in Table S3. Mutagenesis of *SH3P1* and *SH3P2* was performed in Col-0 background using SH3P-A CRISPR/pHEE401 and in *sh3p3* background using SH3P-B CRISPR/pHEE401. Mutagenesis of TASH3 was performed in Col-0 and in *sh3p123*^{10G} backgrounds independently but identical mutant allele *tash3-c* was isolated. In T1 plants, target sequences were PCR-amplified and sequenced using primers listed in Table S2. Where homozygotes were not found, further genotyping was performed in T2 generation. Plants negative for the CRISPR/Cas9 transgene were selected in T2 generation by PCR on *Cas9* gene sequence. Details of generated mutant alleles are given in Table S1.

Quantitative reverse transcriptase PCR

Total RNA was isolated from 5 day old seedlings using RNeasy Plant Mini Kit (Qiagen). cDNA was synthetised using iScript cDNA Synthesis Kit (Bio-Rad). qPCR was performed with Luna reagent (New England Biolabs) in Roche LightCycler 480. *TUB2* and *PP2AA3* were used as reference genes. Primer sequences are listed in Table S2.

Accession numbers

The Arabidopsis Genome Initiative (AGI) locus codes of genes used in this study are: SH3P1 (AT1G31440), SH3P2 (AT4G34660), SH3P3 (AT4G18060), TASH3 (AT2G07360), AUXILIN-LIKE1 (AT4G12780), CLC2 (AT2G40060).

QUANTIFICATION AND STATISTICAL ANALYSIS

Details of all quantification and statistical analyses, such as statistical tests used, significance, exact values of n and their definition, and definition of dispersion measures, are given in Figure legends. Seedling root lengths were measured in Fiji (https://imagej.net/Fiji). Measurements of relative PM signal intensities of SH3P2-GFP and mCherry-AUXILIN-LIKE1 on CLSM images were performed in Fiji as a ratio between mean gray value of a line drawn over multiple PMs in each CLSM image, and a rectangle covering the total visible RAM area. Quantifications of FM4-64 uptake were performed in Fiji as a ratio between mean gray value of a line drawn over multiple PMs in each CLSM image, and a region of interest (ROI) consisting of interiors of corresponding cells. BFA body diameters were measured from CLSM images using Fiji. For TIRF imaging, foci density, foci diameter, and event lifetime quantifications were performed using Fiji. To calculate foci density, CLC2-GFP and SH3P2-GFP foci were counted in representative square regions of 36 μm^2 taken from the captured TIRF images or movies. Depending on the experiment, a single region of interest was quantified from each seedling, or from each captured cell, as described in Figure legends. Lifetimes of CLC2-GFP as well as of SH3P2-GFP recruited to CLC2-mRu-positive CCVs were measured in kymographs extracted from the captured TIRF movies by Reslice function in Fiji.